

Supersolid-like states in a two-dimensional trapped spin-orbit-coupled spin-1 condensate

S. K. Adhikari*

Instituto de Física Teórica, Universidade Estadual Paulista - UNESP, 01.140-070 São Paulo, São Paulo, Brazil

(Dated: April 7, 2021)

We study supersolid-like states in a quasi-two-dimensional trapped Rashba and Dresselhaus spin-orbit (SO) coupled spin-1 condensate. For small strengths of SO coupling γ ($\gamma \lesssim 0.75$), in the ferromagnetic phase, circularly-symmetric $(0, \pm 1, \pm 2)$ - and $(\mp 1, 0, \pm 1)$ -type states are formed where the numbers in the parentheses denote the angular momentum of the vortex at the center of the components and where the upper (lower) sign correspond to Rashba (Dresselhaus) coupling; in the antiferromagnetic phase, only $(\mp 1, 0, \pm 1)$ -type states are formed. For large strengths of SO coupling, supersolid-like superlattice and superstripe states are formed in the ferromagnetic phase. In the antiferromagnetic phase, for large strengths of SO coupling, supersolid-like superstripe and multi-ring states are formed. For an equal mixture of Rashba and Dresselhaus SO couplings, only a superstripe state is found. All these states are found to be dynamically stable and hence accessible in an experiment and will enhance the fundamental understanding of crystallization onto spatially periodic states in solids.

1. INTRODUCTION

After the experimental realization [1] of a trapped Bose-Einstein condensate (BEC) of ultra-dilute alkali metal atoms at ultra-low temperature, it has been possible to observe a hyperfine spin-1 ($F = 1$) spinor BEC of ^{23}Na atoms composed of the three spin components $F_z = \pm 1, 0$ [2]. The spin-orbit (SO) coupling naturally appears in charged electrons and controls many properties of a solid including its crystalline or amorphous structure. Although, in a neutral atom, there cannot be a natural SO coupling, it is possible to introduce an artificial synthetic SO coupling by Raman lasers that coherently couple the spin-component states in a spinor BEC [3]. Two possible SO couplings are due to Dresselhaus [4] and Rashba [5]. An equal mixture of these SO couplings has been realized in a pseudo spin-1/2 ^{87}Rb [6] and in a ^{23}Na [7] BEC containing only two spin components $F_z = 0, -1$ of total spin $F = 1$ and in a spin-1 ferromagnetic ^{87}Rb BEC, containing all three spin components $F_z = \pm 1, 0$ [8]. There has also been study of SO coupling in a fermionic system [9]. A spin-1 spinor BEC [2] appears in two magnetic phases [10] with distinct properties: ferromagnetic ($a_0 > a_2$) and antiferromagnetic ($a_0 < a_2$), where a_0 and a_2 are the scattering lengths in the total spin 0 and 2 channels, respectively.

A supersolid [11] is a quantum state where matter forms a spatially-ordered stable structure as in a crystalline solid, breaking continuous translational invariance, and enjoys friction-less flow as in a superfluid, breaking continuous gauge invariance. Hence a supersolid simultaneously possesses qualities of a solid and a

superfluid, contrary to the intuition that friction-less flow is a property exclusive to quantum fluids, e.g. Fermi superfluids [12], and BECs [1]. There have been theoretical suggestion for supersolid-like states in an SO-coupled BEC [13]. Recently, there has been experimental confirmation of a periodic one-dimensional (1D) superstripe state with density modulation in an SO-coupled pseudo spin-1/2 spinor BEC of ^{23}Na atoms [14] employing an equal mixture of Rashba and Dresselhaus couplings. Following theoretical suggestions to create a supersolid with dipolar [15] and finite-range [16] atomic interactions, more recently, different experimental groups also confirmed its presence in a dipolar BEC in quasi-two-dimensional (quasi-2D) [17] and quasi-1D [18] geometries.

In this paper, we demonstrate the appearance of supersolid-like spatially-periodic states in a harmonically-trapped quasi-2D Rashba or Dresselhaus SO-coupled spin-1 BEC in both ferromagnetic and antiferromagnetic phases. In the ferromagnetic phase, the supersolid-like state is an excited state. The ground state for all strengths γ of SO coupling in the ferromagnetic phase is a circularly-asymmetric state without internal vortex. In addition, for a small strength γ ($\lesssim 0.75$) of SO coupling, one has the formation of circularly-symmetric $(\mp 1, 0, \pm 1)$ - and $(0, \pm 1, \pm 2)$ -type states [19], where the numbers in the parentheses denote the angular momentum of vortices at the center of the respective components $F_z = +1, 0, -1$: the upper (lower) sign corresponds to Rashba (Dresselhaus) coupling and the negative sign denotes an anti-vortex of opposite vorticity. For larger SO coupling ($\gamma \gtrsim 0.75$), one encounters two types of supersolid-like states in the ferromagnetic phase: (i) a state with an 1D periodic stripe in density and (ii) a spontaneous crystallization onto a 2D square-lattice state. In the antiferromagnetic phase, there is no circularly-asymmetric state. For a

*s.k.adhikari@unesp.br

<https://professores.ift.unesp.br/sk.adhikari/>

small γ ($\lesssim 0.75$), one encounters a circularly-symmetric ($\mp 1, 0, \pm 1$)-type state [19] in the antiferromagnetic phase. For larger SO coupling ($\gamma \gtrsim 0.75$), two types of supersolid-like states are found: (i) a state with an 1D periodic stripe in density and (ii) a state with a radially-periodic multi-ring pattern in density. For an equal mixture of Rashba and Dresselhaus SO couplings, the only possible spatially-periodic state is the 1D stripe state appearing in both ferromagnetic and antiferromagnetic phases, in addition to a circularly-symmetric Gaussian-type state in the ferromagnetic phase; no other supersolid-like state is found. In the ferromagnetic phase, the circularly-symmetric state is the ground state. These spatially-periodic states in an SO-coupled BEC, sharing some properties of a supersolid, have their own names [20], e.g., superstripe [21] and superlattice [22] states. A superstripe state has an 1D periodic pattern in density, whereas a superlattice state has a 2D periodic square-lattice pattern in density. In a quasi-1D and a quasi-2D uniform SO-coupled spin-1 spinor BEC, superstripe [23] and superlattice [22] states have also been predicted.

In section 2 we present the mean-field model which we solve numerically to study the formation of spatially-periodic states in a harmonically-trapped SO-coupled spin-1 BEC. In section 3 we present numerical results for the formation of spatially-periodic states in a quasi-2D SO-coupled spin-1 BEC for Rashba, Dresselhaus couplings, and for an equal mixture of these couplings, employing imaginary-time propagation. The dynamical stability of the spatially-periodic states are established by real-time propagation using the converged imaginary-time wave function as the initial state. Finally, in section 4 a summary of the findings is presented.

2. MEAN-FIELD MODEL FOR SO-COUPLED SPIN-1 BEC

We consider a BEC of N atoms, each of mass M , under a quasi-2D harmonic trap $V(\mathbf{r}) = M\omega^2(x^2 + y^2)/2 + M\omega_z^2 z^2/2$ ($\omega_z \gg \omega$), where ω and ω_z are the angular trap frequencies in the $x - y$ plane and in the z direction, respectively. The single-particle Hamiltonian of the three-dimensional (3D) SO-coupled BEC is [10]

$$H_0 = -\frac{\hbar^2}{2M}(\nabla_{\rho}^2 + \partial_z^2) + \frac{M}{2}[\omega^2(x^2 + y^2) + \omega_z^2 z^2] + H_{\text{SO}}, \quad (1)$$

where $\boldsymbol{\rho} \equiv \{x, y\}$, $\nabla_{\rho}^2 \equiv (\partial_x^2 + \partial_y^2)$, $\partial_x \equiv \partial/\partial x$, $\partial_y \equiv \partial/\partial y$, $\partial_z \equiv \partial/\partial z$. The SO-coupling interaction is [6, 24]

$$H_{\text{SO}} = \gamma(\nu p_y \Sigma_x - p_x \Sigma_y), \quad (2)$$

where $\nu = +1, -1, 0$, respectively, for Rashba and Dresselhaus SO couplings, and an equal mixture of these SO couplings, γ is the strength of SO coupling, the x and

y components of the momentum operator, respectively, $p_x = -i\hbar\partial_x$, $p_y = -i\hbar\partial_y$, and the irreducible representations of the x and y components of the spin matrices Σ_x and Σ_y are

$$\Sigma_x = \frac{1}{\sqrt{2}} \begin{pmatrix} 0 & 1 & 0 \\ 1 & 0 & 1 \\ 0 & 1 & 0 \end{pmatrix}, \quad \Sigma_y = \frac{i}{\sqrt{2}} \begin{pmatrix} 0 & -1 & 0 \\ 1 & 0 & -1 \\ 0 & 1 & 0 \end{pmatrix}. \quad (3)$$

The reduced quasi-2D coupled Gross-Pitaevskii (GP) equation [25] of the three spin components, for the SO-coupled spin-1 spinor BEC, is [10]

$$i\partial_t \psi_{\pm 1}(\boldsymbol{\rho}) = [\mathcal{H} + c_2(n_{\pm 1} - n_{\mp 1} + n_0)]\psi_{\pm 1}(\boldsymbol{\rho}) + \{c_2\psi_0^2(\boldsymbol{\rho})\psi_{\mp 1}^*(\boldsymbol{\rho})\} - i\tilde{\gamma}(\nu\partial_y \pm i\partial_x)\psi_0(\boldsymbol{\rho}), \quad (4)$$

$$i\partial_t \psi_0(\boldsymbol{\rho}) = [\mathcal{H} + c_2(n_{+1} + n_{-1})]\psi_0(\boldsymbol{\rho}) + \{2c_2\psi_{+1}(\boldsymbol{\rho}) \times \psi_{-1}(\boldsymbol{\rho})\psi_0^*(\boldsymbol{\rho})\} - i\tilde{\gamma}[-i\partial_x\phi_-(\boldsymbol{\rho}) + \nu\partial_y\phi_+(\boldsymbol{\rho})], \quad (5)$$

$$\mathcal{H} = -\frac{1}{2}\nabla_{\rho}^2 + \frac{1}{2}\rho^2 + c_0 n, \quad (6)$$

$$c_0 = \frac{2N\sqrt{2\pi\kappa}(a_0 + 2a_2)}{3}, \quad c_2 = \frac{2N\sqrt{2\pi\kappa}(a_2 - a_0)}{3}, \quad (7)$$

where $\kappa = \omega_z/\omega$, $\phi_{\pm}(\boldsymbol{\rho}) = \psi_{+1}(\boldsymbol{\rho}) \pm \psi_{-1}(\boldsymbol{\rho})$, $\partial_t \equiv \partial/\partial t$, $\tilde{\gamma} = \gamma/\sqrt{2}$, $n_j = |\psi_j|^2$, $j = \pm 1, 0$ are the densities of spin components $F_z = \pm 1, 0$, $n(\boldsymbol{\rho}) = \sum_j n_j(\boldsymbol{\rho})$ the total density, and the asterisk denotes complex conjugate. All quantities in (4)-(7) and in the following are dimensionless; this is achieved by expressing lengths (a_0, a_2, x, y, z) in units of oscillator length $l_0 \equiv \sqrt{\hbar/M\omega}$, energy in units of $\hbar\omega$, density in units of l_0^{-2} , and time in units of ω^{-1} . In ferromagnetic and antiferromagnetic phases $c_2 < 0$, and $c_2 > 0$, respectively, and the normalization condition is $\int n(\boldsymbol{\rho}) d^2\rho = 1$. The single-particle quasi-2D Hamiltonian corresponding to (4) and (5) is given by

$$H_{2\text{D}} = -\frac{1}{2}\nabla_{\rho}^2 + \frac{1}{2}\rho^2 + H_{\text{SO}}. \quad (8)$$

The energy functional for the time-independent version of (4)-(5) is

$$E[\psi] = \frac{1}{2}\int d^2\rho [\sum_j |\nabla_{\rho}\psi_j|^2 + \rho^2 n + c_0 n^2 + c_2\{n_{+1}^2 + n_{-1}^2 + 2(n_{+1}n_0 + n_{-1}n_0 - n_{+1}n_{-1}) + \psi_{-1}^*\psi_0^2\psi_{+1}^* + \psi_{-1}\psi_0^{*2}\psi_{+1}\}] - 2i\tilde{\gamma}\{\nu\psi_0^*\partial_y\phi_+ + \nu\phi_+^*\partial_y\psi_0 - i\psi_0^*\partial_x\phi_- + i\phi_-^*\partial_x\psi_0\}. \quad (9)$$

3. NUMERICAL RESULTS

We solve (4) and (5) numerically by time propagation, after a discretization using the split-time-step Crank-Nicolson discretization rule [26] employing a space step of 0.1 and a time step of 0.001 for imaginary-time propagation and 0.00025 for real-time propagation. The lowest-energy stationary solutions of each type of symmetry are obtained by imaginary-time propagation. The

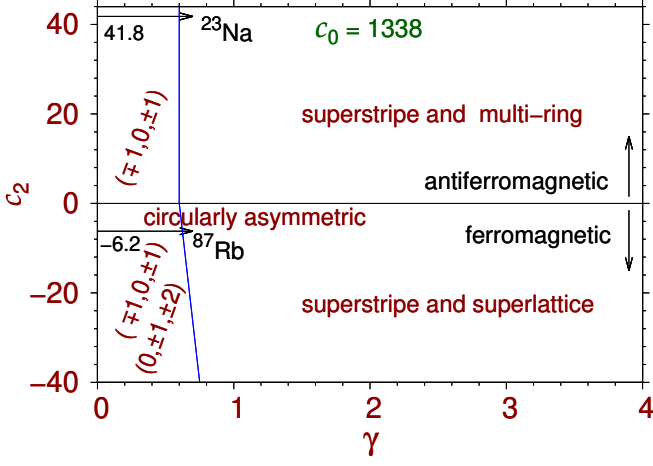


FIG. 1: The c_2 versus γ phase plot for Rashba and Dresselhaus SO couplings showing different types of possible states in different regions of parameter space for $c_0 = 1338$. Results in all figures are in dimensionless units.

dynamical stability of a state is then tested by real-time propagation employing the converged imaginary-time wave function as the initial state. The normalization is held fixed during time propagation. Magnetization $m = \int d^2\rho [n_{+1}(\rho) - n_{-1}(\rho)]$ is not a conserved quantity and is allowed to evolve freely during time propagation to attain a final converged value.

Instead of presenting the results in dimensionless units, we prefer to relate the results with the most commonly used ferromagnetic ^{87}Rb and antiferromagnetic ^{23}Na atoms with the following scattering lengths, respectively: for ^{87}Rb [27] $a_0 = 101.8a_B$, $a_2 = 100.4a_B$ and for ^{23}Na [28] $a_0 = 50.0a_B$, and $a_2 = 55.0a_B$, with $a_B (= 5.291772 \times 10^{-11} \text{ m})$ the Bohr radius. In the ferromagnetic phase we present results for a harmonically trapped quasi-2D spin-1 ^{87}Rb BEC of $N = 10^5$ atoms with $l_0/\sqrt{\kappa} = 2 \mu\text{m}$ so that $c_0 \equiv 2N\sqrt{2\pi\kappa}(a_0 + 2a_2)/3l_0 \approx 1338$ and $c_2 \equiv 2N\sqrt{2\pi\kappa}(a_2 - a_0)/3l_0 \approx -6.2$. In the antiferromagnetic phase we consider a harmonically trapped quasi-2D spin-1 ^{23}Na BEC of $N = 1.891 \times 10^5$ atoms so that $c_0 \equiv 2N\sqrt{2\pi\kappa}(a_0 + 2a_2)/3l_0 \approx 1338$ and $c_2 \equiv 2N\sqrt{2\pi\kappa}(a_2 - a_0)/3l_0 \approx 41.8$. The number of atoms are so chosen so as to have the same c_0 in both cases. In this fashion we keep c_0 fixed at 1338 and change c_2 continuously from -6.2 to 41.8 to cover both ferromagnetic and antiferromagnetic phases from ^{87}Rb to ^{23}Na . This choice will allow a unified description of the ferromagnetic ^{87}Rb and antiferromagnetic ^{23}Na phases, viz. Figs. 1, 2(m)-(o), 4(g)-(i), etc.

The scenario of the formation of different types of states – a circularly asymmetric state, circularly-symmetric $(0, \pm 1, \pm 2)$ - and $(\mp 1, 0, \pm 1)$ -type states, superstripe, multi-ring, and superlattice states – for Rashba and Dresselhaus SO couplings in the ferromagnetic and antiferromagnetic phases is illustrated in fig-

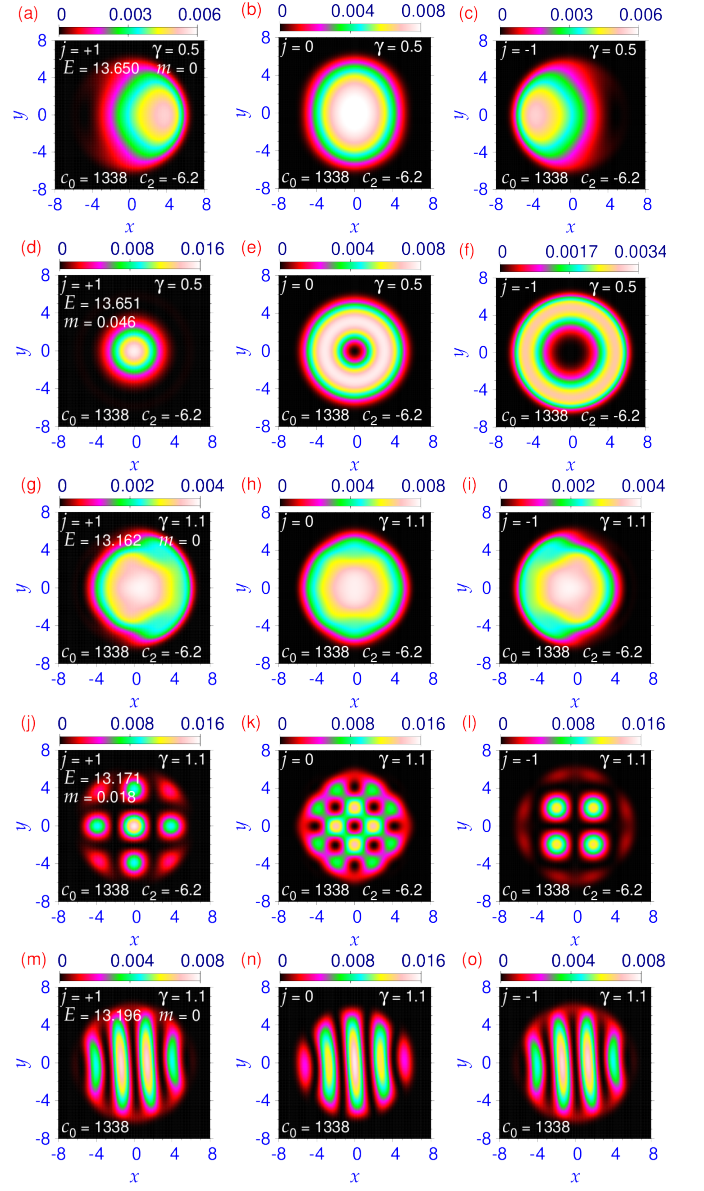


FIG. 2: Contour plot of density $n_j(\rho)$ of a circularly-asymmetric Rashba or Dresselhaus SO-coupled ferromagnetic ^{87}Rb BEC for $\gamma = 0.5$ of components (a) $j = +1$, (b) $j = 0$ and (c) $j = -1$; the same of a circularly-symmetric $(0, \pm 1, \pm 2)$ -type Rashba or Dresselhaus SO-coupled BEC for $\gamma = 0.5$ in (d) $j = +1$, (e) $j = 0$ and (f) $j = -1$; the same of a circularly-asymmetric Rashba or Dresselhaus SO-coupled ferromagnetic ^{87}Rb BEC for $\gamma = 1.1$ of components (g) $j = +1$, (h) $j = 0$ and (i) $j = -1$; the same of a superlattice SO-coupled ferromagnetic ^{87}Rb BEC for $\gamma = 1.1$, in (j)-(l); the same of a superstripe SO-coupled ferromagnetic ^{87}Rb or antiferromagnetic ^{23}Na BEC for $\gamma = 1.1$, in (m)-(o). The superstripe phase presented in (m)-(o) is independent of c_2 . The energy E and magnetization m are displayed in the plot of the $j = +1$ component in figures 2, 4, 5, and 6.

ure 1 through a $c_2 - \gamma$ phase plot for $c_0 = 1338$. In the ferromagnetic phase ($c_2 < 0$), for all values of SO-coupling strength γ , the lowest-energy state is a

circularly-asymmetric localized state without any internal vortex. In addition, for a small γ ($\gamma \lesssim 0.75$) one can have either a circularly-symmetric $(0, \pm 1, \pm 2)$ -type state or an excited circularly-symmetric $(\mp 1, 0, \pm 1)$ -type state. For large γ , in the ferromagnetic phase we have either a superlattice state with periodic square-lattice pattern in density or a superstripe state with an 1D stripe in density. In the antiferromagnetic phase ($c_2 > 0$), there is no circularly-asymmetric localized state, and for a small γ ($\gamma \lesssim 0.75$), one can have a circularly-symmetric $(\mp 1, 0, \pm 1)$ -type state. For large γ , in the antiferromagnetic phase, in addition to the 1D superstripe state, it is possible to have a multi-ring state with radially-periodic multi-ring pattern in density.

We study the formation of the different types of states by a numerical solution of (4) and (5), by imaginary-time propagation, in a Rashba or Dresselhaus SO-coupled ferromagnetic ^{87}Rb BEC with $c_0 = 1338$ and $c_2 = -6.2$. For $\gamma = 0.5$, we find the quasi-degenerate circularly-asymmetric state as the ground state and the circularly-symmetric $(0, \pm 1, \pm 2)$ -type state. In figures 2(a)-(c) we illustrate the circularly-asymmetric state through a contour plot of density of the components $j = +1, 0$ and $j = -1$ for $\gamma = 0.5$, respectively, obtained by using a localized state without vortices as the initial wave function. The energy E and magnetization m of the states are displayed in the contour density plot of component $j = +1$. The numerical value of magnetization of all states presented in this paper are zero except the states in figures 2(d)-(f) and 2(j)-(l). In figures 2(d)-(f), we display the component densities of the circularly-symmetric $(0, \pm 1, \pm 2)$ -type state for $\gamma = 0.5$. To simulate the $(0, \pm 1, \pm 2)$ -type state, in imaginary-time propagation, the vortices of angular momenta ± 1 and ± 2 were imprinted in components $j = 0$ and $j = -1$ of the localized initial wave function. The central hole in components $j = 0, -1$ of figures 2(e)-(f) corresponds to the core of vortices/anti-vortices of angular momenta $\pm 1, \pm 2$, respectively. Although the densities of the Rashba and Dresselhaus SO-coupled states are the same, their phases are different. The contour plot of the phase of the wave function components $j = +1, 0, -1$ of the Rashba SO-coupled state of figures 2(a)-(c) is shown in figures 3(a)-(c); the same of the Dresselhaus SO-coupled state is shown in figures 3(d)-(f). The phase drops upon a complete rotation in plots 3(b)-(c) for Rashba SO coupling are 2π and 4π indicating angular momenta of $+1$ and $+2$ in these components. The corresponding angular momenta of components $j = 0$ and $j = -1$ from figures 3(e)-(f) for Dresselhaus SO coupling are -1 and -2 . The energies of the circularly-asymmetric and the $(0, \pm 1, \pm 2)$ -type states for $\gamma = 0.5$ shown in figures 2(a)-(c) and 2(d)-(f) are $E = 13.650$ and 13.651 , respectively. In this case there is also a $(\mp 1, 0, \pm 1)$ -type excited state with energy $E = 13.681$, appearing in both ferromagnetic and

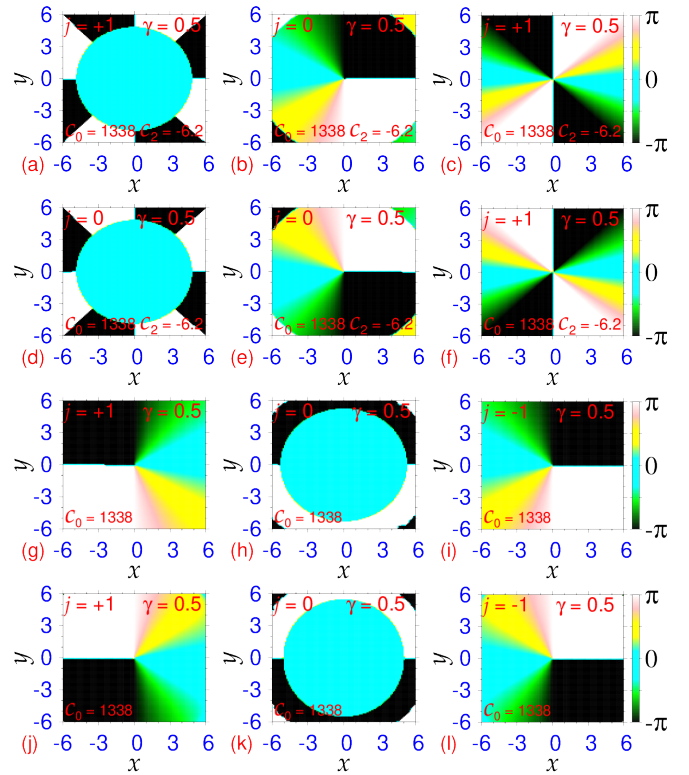


FIG. 3: The contour plot of the phase of the wave function of the $(0, +1, +2)$ -type Rashba SO-coupled ferromagnetic BEC of figures 2(d)-(f) of components (a) $j = +1$, (b) $j = 0$, and (c) $j = -1$; the same of the $(0, -1, -2)$ -type Dresselhaus SO-coupled ferromagnetic BEC of figures 2(d)-(f) of components (d) $j = +1$, (e) $j = 0$, and (f) $j = -1$; the same of the $(-1, 0, +1)$ -type Rashba SO-coupled BEC of figures 5(a)-(c) of components (g) $j = +1$, (h) $j = 0$ and (i) $j = -1$; the same of a $(+1, 0, -1)$ -type Dresselhaus SO-coupled BEC figures 5(a)-(c) of components (g) $j = +1$, (h) $j = 0$ and (i) $j = -1$.

antiferromagnetic phases, viz. figures 5(a)-(c).

As γ is increased, the circularly-asymmetric state continues to exist in the ferromagnetic phase as the ground state, but the $(0, \pm 1, \pm 2)$ -type state evolves into a superlattice state with a periodic square-lattice pattern in density; the $(\mp 1, 0, \pm 1)$ -type state simply cease to exist. The single-particle Hamiltonian (8) should have solutions of the plane wave form $\exp(\pm i\gamma x) \times \exp(\pm i\gamma y)$ or of the form $\exp(\pm i\gamma\rho)$. In the presence of interaction ($c_0, c_2 \neq 0$), the solution will be a superposition of such plane wave solutions leading to a periodic variation of density in the form $\sin^2(\gamma x)$, $\cos^2(\gamma y)$, $\sin^2(\gamma x) \sin^2(\gamma y)$, $\sin^2(\gamma\rho)$ etc. appropriate for superstripe, superlattice or multi-ring BECs, respectively. This has been demonstrated in detail for quasi-1D SO-coupled BEC [29], the same of the present quasi-2D SO-coupled BEC will be the subject of a future investigation. Although superstripe, superlattice and multi-ring states are possible from a con-

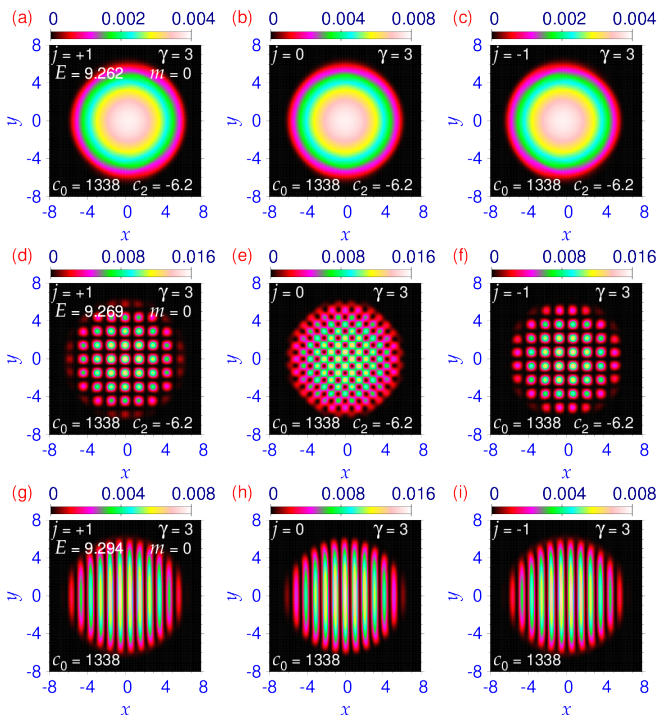


FIG. 4: Contour plot of density $n_j(\boldsymbol{\rho})$ of a circularly-asymmetric Rashba or Dresselhaus SO-coupled ferromagnetic ^{87}Rb BEC for $\gamma = 3$ of components (a) $j = +1$, (b) $j = 0$ and (c) $j = -1$; the same of a superlattice Rashba or Dresselhaus SO-coupled BEC for $\gamma = 3$ of components (d) $j = +1$, (e) $j = 0$ and (f) $j = -1$; the same of a superstripe Rashba or Dresselhaus SO-coupled ferromagnetic ^{87}Rb or an antiferromagnetic ^{23}Na BEC for $\gamma = 3$ of components (g) $j = +1$, (h) $j = 0$ and (i) $j = -1$. In plots (a)-(f) $c_0 = 1338$, $c_2 = -6.2$; the profile in plots (g)-(i) is for $c_0 = 1338$ and independent of c_2 thus holding for both ferromagnetic and antiferromagnetic phases.

sideration of the mean-field GP equation, for certain parameter domain one of these becomes the ground state, the others could appear as excited states or could even be unstable. For example, we will see that, in the antiferromagnetic phase, the superstripe state is the ground state, the multi-ring state is an excited state, viz. figures 4(g)-(i) and 5, and the superlattice state is unstable. However, we established in [22] that in a *uniform* spin-1 SO-coupled BEC the superlattice state can appear in both ferromagnetic as well as antiferromagnetic phases. In the ferromagnetic phase, the circularly asymmetric state is the ground state, viz. figure 2.

Using the converged circularly-symmetric $(0, \pm 1, \pm 2)$ -type wave function for $\gamma = 0.5$ as the initial state in imaginary-time propagation, we find the superlattice state for larger γ ($\gamma \gtrsim 0.75$), while the circular symmetry is spontaneously broken and the formation of superlattice states for $\gamma = 1.1$ are illustrated through a contour plot of densities of components $j = +1, 0$ and $j = -1$,

respectively, in figures 2(g)-(i) and (j)-(l) with energies $E = 13.162$ and 13.171 . In addition, there is the excited superstripe state with energy 13.196 displayed in figures 2(m)-(o). The energy and density of this superstripe state is independent of c_2 (in the range $40 > c_2 > -40$) and hence is the same in both ferromagnetic and antiferromagnetic phases. In the numerical simulation, the stripe pattern is imprinted on the initial state as: $\psi_{\pm 1}(\boldsymbol{\rho}) \sim \sin(\gamma x)\psi_{\text{loc}}(\boldsymbol{\rho})$, $\psi_0(\boldsymbol{\rho}) \sim \cos(\gamma x)\psi_{\text{loc}}(\boldsymbol{\rho})$, where $\psi_{\text{loc}}(\boldsymbol{\rho})$ is a localized normalizable state.

With the increase of SO coupling $\gamma (= 3)$, in the ferromagnetic phase the circularly asymmetric state continues as the ground state ($E = 9.262$), with reduced asymmetry, as shown in figures 4(a)-(c), where we plot the contour densities of components $j = +1, 0, -1$, respectively. The superstripe state for the same parameters as displayed in figures 4(d)-(f) for $\gamma = 3$ ($E = 9.269$) is an excited state. In this state, the square-lattice pattern has become more prominent with the increase of γ . For all γ , the square lattice for the $j = 0$ component makes an angle of 45° with the square lattice for $j = \pm 1$ components and there is no symmetry between densities of $j = \pm 1$ components. As γ increases, the array of lattices in the spatially-periodic state is denser and the number of occupied sites increases, although the size of the condensate does not increase: the size is controlled by the external trap. The profile of the superstripe state with $\gamma = 3$, $c_0 = 1338$ is shown in figures 4(g)-(i). The energy and density of this superstripe state are independent of c_2 ; hence the results are valid for both ferromagnetic and antiferromagnetic phases. However, the superstripe state ($E = 9.294$) is an excited state in the ferromagnetic phase, whereas it is the ground state in the antiferromagnetic phase. The result of densities and energies for Rashba and Dresselhaus SO couplings are the same, although the underlying wave functions are different.

Now we consider the formation of a spatially-periodic state in an antiferromagnetic SO-coupled spin-1 ^{23}Na BEC with $c_0 = 1338$ and $c_2 = 41.8$. For a small γ ($\gamma \lesssim 0.75$), the only possible state is a circularly-symmetric $(\mp 1, 0, \pm 1)$ -type state [19], for Rashba and Dresselhaus SO couplings, respectively, as displayed in the contour density plot of figures 5(a)-(c) for $\gamma = 0.5$. In imaginary-time propagation, the vortices of angular momenta ∓ 1 (± 1) were imprinted in components $j = \pm 1$ of the initial wave function. The energy ($E = 13.681$) and density of this state are independent of c_2 ; hence the results are valid for both antiferromagnetic and ferromagnetic phases for weak SO coupling ($\gamma \lesssim 0.75$). However, the $(\mp 1, 0, \pm 1)$ -type state is an excited state in the ferromagnetic phase, whereas it is the ground state in the antiferromagnetic phase. The phases of the wave function for Rashba and Dresselhaus SO couplings are different. In figures 3(g)-(i) and 3(j)-(l) we illustrate the contour plot of the phases of the wave function compo-

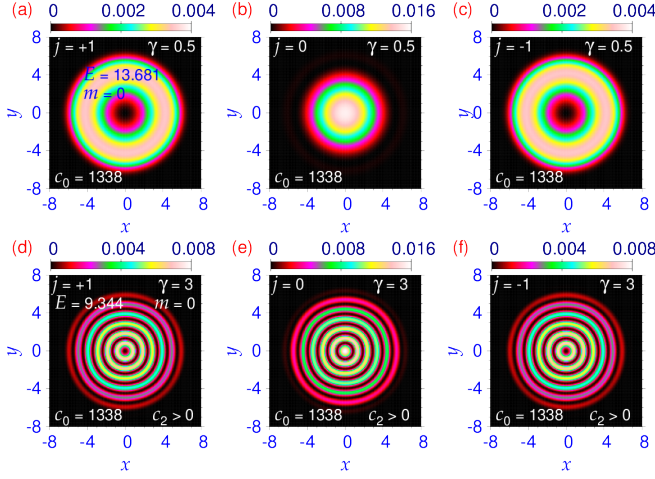


FIG. 5: Contour plot of density $n_j(\rho)$ of a circularly-symmetric $(\mp 1, 0, \pm 1)$ -type Rashba or Dresselhaus SO-coupled antiferromagnetic ^{23}Na or ferromagnetic ^{87}Rb BEC for $\gamma = 0.5$ of components (a) $j = +1$, (b) $j = 0$ and (c) $j = -1$; the same of a circularly-symmetric multi-ring Rashba or Dresselhaus SO-coupled antiferromagnetic ^{23}Na BEC for $\gamma = 3$ of components (d) $j = +1$, (e) $j = 0$ and (f) $j = -1$. In all plots $c_0 = 1338$, $c_2 = 41.8$

nents $j = +1, 0, -1$ for the BECs of figures 5(a)-(c) for Rashba and Dresselhaus couplings, respectively. These phase plots confirm the angular momenta of ∓ 1 and ± 1 in components $j = \pm 1$ for Rashba and Dresselhaus couplings, respectively. Using the converged wave function for $\gamma = 0.5$ as the initial state, we obtain the multi-ring state for larger values of γ , by increasing γ slowly during imaginary-time propagation, as illustrated in figures 5(d)-(f) for $\gamma = 3$ in the contour density plot of the components $j = +1, 0, -1$. The anti-vortex and vortex at the center of the components $j = \pm 1$ of figures 5(a) and (c) survive in figures 5(d) and (f). For $\gamma = 3$ the ground state in the antiferromagnetic phase is the superstripe state, which can be obtained by imaginary-time propagation using an initial Gaussian state with periodic stripe modulation, as shown in figures 4(g)-(i). This state is an excited state in the ferromagnetic phase. In ^{23}Na with $c_0 = 1338$ and $c_2 = 41.8$, of the two types of periodic states the superstripe state ($E = 9.294$), viz. figure 4(g)-(i), has the smaller energy than the multi-ring state ($E = 9.344$), viz. figure 5(d)-(f). The energy of the multi-ring state is independent of the nonlinearity c_2 ($c_2 > 0$).

For an equal mixture of Rashba and Dresselhaus SO couplings a superstripe state is possible in both ferromagnetic and antiferromagnetic phases [13, 14]. In the antiferromagnetic phase the superstripe state is the only possible state. In the ferromagnetic phase, a circularly-symmetric vortex-free state appears as the ground state ($E = 9.296$) as shown through a contour plot of densities of components $j = +1, 0, -1$ in figures 6(a)-(c) for

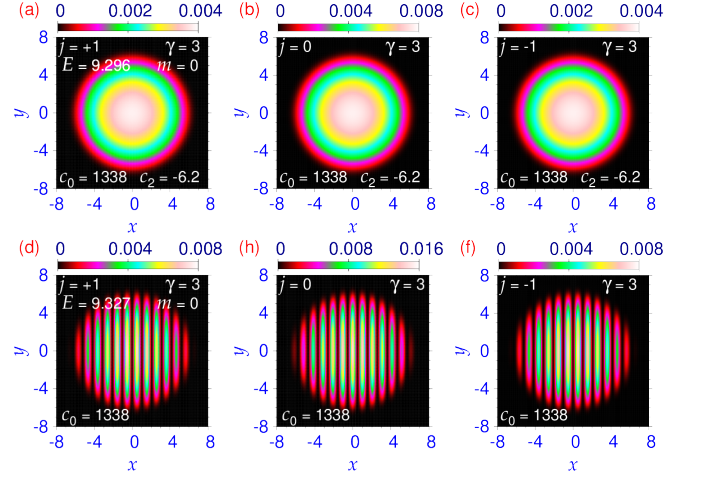


FIG. 6: Contour plot of density $n_j(\rho)$ of a circularly-symmetric ferromagnetic ^{87}Rb BEC for an equal mixture of Rashba and Dresselhaus SO-couplings with $\gamma = 3$ of components (a) $j = +1$, (b) $j = 0$ and (c) $j = -1$; the same of a superstripe ferromagnetic or antiferromagnetic BEC for an equal mixture of Rashba and Dresselhaus SO-couplings with $\gamma = 3$ of components (d) $j = +1$, (e) $j = 0$ and (f) $j = -1$.

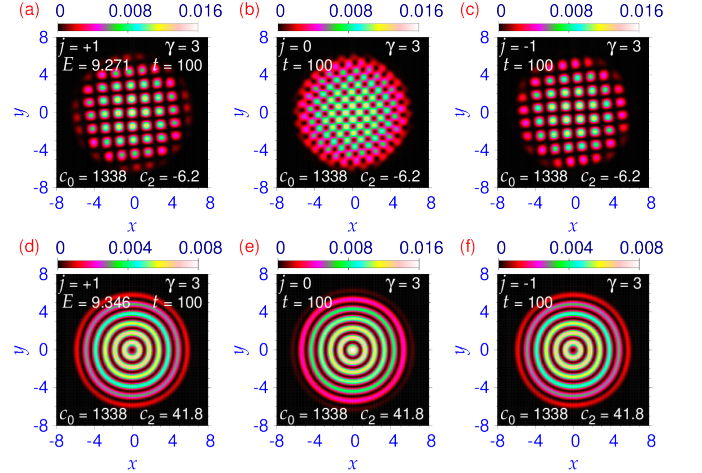


FIG. 7: Contour plot of component densities of the SO-coupled BEC, of figures 2(m)-(o), of components (a) $j = +1$ (b) $j = 0$ and (c) $j = -1$, after real-time propagation during 100 units of time; the same of the SO-coupled BEC, of figures 5(d)-(f), of components (d) $j = +1$ (e) $j = 0$ and (f) $j = -1$, after real-time propagation during 100 units of time. The initial state used in real-time propagation is the corresponding convergent wave function obtained in imaginary-time propagation.

$\gamma = 3$. The superstripe state is illustrated in figures 6(d)-(f). The energy ($E = 9.327$) and the density of the superstripe state is independent of c_2 ; it is an excited state in the ferromagnetic phase.

We test the dynamical stability of the SO-coupled

states considered here via a real-time propagation over an extended period of time using the corresponding convergent wave function obtained in imaginary-time propagation as the initial function. As an illustration we consider the superlattice state of figures 4(d)-(f) and the multi-ring state of figures 5(d)-(f) and subject the corresponding imaginary-time wave functions to real-time propagation during 100 units of time. The resultant densities for the components $j = +1, 0, -1$ are displayed in figures 7(a)-(c), and (d)-(f) respectively. Although the energy and size oscillate during time evolution, the periodic pattern in density survives at $t = 100$, viz. slightly different energies at $t = 100$ ($E = 9.271$ and 9.346) compared to the corresponding converged imaginary-time results ($E = 9.269$ and 9.344). These densities are in good agreement with the corresponding imaginary-time densities, demonstrating the dynamical stability of the spatially-periodic state.

4. SUMMARY

We demonstrated new types of dynamically stable supersolid-like spatially-periodic states in a Rashba or a Dresselhaus SO-coupled harmonically-trapped spin-1 quasi-2D spinor BEC for different SO-coupling strength γ , in both ferromagnetic and antiferromagnetic phases, using a numerical solution of the GP equation. In the ferromagnetic phase, the ground state for all strengths of SO coupling is a circularly-asymmetric localized state without any internal vortex. In the antiferromagnetic phase, there is no circularly-asymmetric localized state. For small strengths of SO coupling ($\gamma \lesssim 0.75$) there is no spatially-periodic state. For small γ , for both Rashba and Dresselhaus SO couplings, in the ferromagnetic phase $(0, \pm 1, \pm 2)$ - and $(\mp 1, 0, \pm 1)$ -type states are found, whereas in the antiferromagnetic phase *only* a $(\mp 1, 0, \pm 1)$ -type state is found. In the ferromagnetic phase, for large strengths of Rashba and Dresselhaus SO couplings ($\gamma \gtrsim 0.75$), the possible spatially-periodic states are superlattice and superstripe states, whereas, in the antiferromagnetic phase, superstripe and multi-ring states are found. A superstripe state was also suggested [15] and observed [14] in a pseudo spin-1/2 ^{23}Na BEC. There has been detailed study [30] of different phases of a trapped SO-coupled quasi-2D pseudo spin-1/2 BEC. The semi-vortex state explored there should in present notation be a $(0, \pm 1)$ -type state with a single vortex/antivortex in one component, quite similar to the $(\mp 1, 0, \pm 1)$ -type state of this paper. Although, no superlattice or superstripe state was reported in that paper [30], a quasi-2D SO-coupled trapped pseudo spin-1/2 BEC is appropriate for hosting a superlattice or superstripe state. The search of such a spatially-periodic state in this system is an interesting topic of future investigation. A superlattice state was first predicted in a quasi-

2D SO-coupled spin-1 uniform BEC [22].

For an equal mixture of Rashba and Dresselhaus couplings, a superstripe state appears in both ferromagnetic and antiferromagnetic phases in addition to a circularly-symmetric Gaussian type state in the ferromagnetic phase. In the ferromagnetic phase the ground state is the circularly-symmetric state. The dynamic stability of these states was established by steady real-time propagation over a long period of time using the converged wave function of imaginary-time calculation as the initial state.

It is remarkable that the superlattice states first found in a uniform system [22] survives under a strong harmonic trap. These states are dynamically robust and deserve further theoretical, and also experimental, investigation. The energy difference between different types of states, e.g. multi-ring state, superstripe state, superlattice state, etc., is very small for experimental measurement. Hence, for experimental purpose, these states for a fixed set of parameters could be considered degenerate. Nevertheless, as all these states are dynamically stable, in an experiment, depending on the initial conditions, any of these quasi-degenerate states could be accessed. A natural extension of this study is to search for spatially-periodic states in an SO-coupled 3D spin-1 and a quasi-2D spin-2 BEC, where a rich variety of spatially-periodic states are expected. It would also be of interest to study the role of the Zeeman-like terms [30] on the present multi-ring, superlattice and superstripe states.

S.K.A. acknowledges support by the CNPq (Brazil) grant 301324/2019-0, and by the ICTP-SAIFR-FAPESP (Brazil) grant 2016/01343-7

-
- [1] M. H. Anderson, J. R. Ensher, M. R. Matthews, C. E. Wieman, and E. A. Cornell, *Science* 269, 198 (1995)
 - [2] K. B. Davis, M.-O. Mewes, M. R. Andrews, N. J. van Druten, D. S. Durfee, D. M. Kurn, and W. Ketterle, *Phys. Rev. Lett.* 75, 3969 (1995)
 - [3] J. Stenger, S. Inouye, D. M. Stamper-Kurn, H.-J. Miesner, A. P. Chikkatur, and W. Ketterle, *Nature* 396, 345 (1998)
 - [4] J. Dalibard, F. Gerbier, G. Juzeliūnas, P. Öhberg, *Rev. Mod. Phys.* 83, 1523 (2011)
 - [5] G. Dresselhaus, *Phys. Rev.* 100, 580 (1955)
 - [6] E. I. Rashba, *Fiz. Tverd. Tela* 2, 1224 (1960) [English Transla.: *Sov. Phys. Solid State* 2, 1109 (1960)]
 - [7] Y.-J. Lin, K. Jiménez-García, I. B. Spielman, *Nature* 471, 83 (2011)
 - [8] J. Li, W. Huang, B. Shteynas, S. Burchesky, F. C. Top, E. Su, J. Lee, A. O. Jamison, and W. Ketterle, *Phys. Rev. Lett.* 117, 185301 (2016)
 - [9] D. Campbell, R. Price, A. Putra, A. Valdés-Curiel, D. Trypogeorgos, and I. B. Spielman, *Nat. Commun.* 7, 10897 (2016)
 - [10] I. V. Tokatly and E. Ya. Sherman *Phys. Rev. A* 87, 041602(R) (2013)

- [10] V. I. Yukalov, *Laser Phys.* 28, 053001 (2018)
Y. Kawaguchi and M. Ueda, *Phys. Rep.* 520, 253 (2012)
S. Gautam and S. K. Adhikari, *Phys. Rev. A* 92, 023616 (2015)
- [11] M. Boninsegni and N. V. Prokof'ev, *Rev. Mod. Phys.* 84, 759 (2012)
A. F. Andreev and I. M. Lifshitz, *Zh. Eksp. Teor. Fiz.* 56, 2057 (1969) [English Transla.: *Sov. Phys. JETP* 29, 1107 (1969)]
E.P. Gross, *Phys. Rev.* 106, 161 (1957)
A. J. Leggett, *Phys. Rev. Lett.* 25, 1543 (1970)
G. V. Chester, *Phys. Rev. A* 2, 256 (1970)
V. I. Yukalov, *Physics* 2, 49 (2020)
- [12] M. W. Zwierlein, C. H. Schunck, A. Schirotzek, and W. Ketterle, *Nature* 442, 54 (2006)
M. Greiner, C. A. Regal, and D. S. Jin, *Nature* 426, 537 (2003)
- [13] T.-L. Ho and S. Zhang, *Phys. Rev. Lett.* 107, 150403 (2011)
R. Liao, *Phys. Rev. Lett.* 120, 140403 (2018)
W. Han, X.-F. Zhang, D.-S. Wang, H.-F. Jiang, W. Zhang, and S.-G. Zhang, *Phys. Rev. Lett.* 121, 030404 (2018)
- [14] J.-R. Li, J. Lee, W. Huang, S. Burchesky, B. Shteynas, F. Ç. Top, A. O. Jamison, and W. Ketterle, *Nature* 543, 91 (2017)
- [15] R. Bombin, J. Boronat, and F. Mazzanti, *Phys. Rev. Lett.* 119, 250402 (2017)
Zhen-Kai Lu, Yun Li, D. S. Petrov, and G. V. Shlyapnikov, *Phys. Rev. Lett.* 115, 075303 (2015)
N. Y. Yao, C. R. Laumann, A. V. Gorshkov, S. D. Bennett, E. Demler, P. Zoller, and M. D. Lukin, *Phys. Rev. Lett.* 109, 266804 (2012)
- [16] G. Masella, A. Angelone, F. Mezzacapo, G. Pupillo, and N. V. Prokof'ev, *Phys. Rev. Lett.* 123, 045301 (2019)
F. Cinti, P. Jain, M. Boninsegni, A. Micheli, P. Zoller, and G. Pupillo, *Phys. Rev. Lett.* 105, 135301 (2010)
S. Saccani, S. Moroni, and M. Boninsegni, *Phys. Rev. Lett.* 108, 175301 (2012)
- [17] F. Böttcher, J.-N. Schmidt, M. Wenzel, J. Hertkorn, M. Guo, T. Langen, T. Pfau, *Phys. Rev. X* 9, 011051 (2019)
J. Hertkorn, F. Böttcher, M. Guo, J. N. Schmidt, T. Langen, H. P. Büchler, T. Pfau, *Phys. Rev. Lett.* 123, 193002 (2019)
- [18] L. Tanzi, E. Lucioni, F. Famá, J. Catani, A. Fioretti, C. Gabbanini, R. N. Bisset, L. Santos, G. Modugno, *Phys. Rev. Lett.* 122, 130405 (2019)
S. V. Andreev, *Phys. Rev. B* 95, 184519 (2017)
G. Natale, R. M. W. van Bijnen, A. Patscheider, D. Pette, M. J. Mark, L. Chomaz, F. Ferlaino, *Phys. Rev. Lett.* 123, 050402 (2019)
- [19] T. Mizushima, K. Machida, T. Kita, *Phys. Rev. Lett.* 89, 030401 (2002)
T. Mizushima, K. Machida, T. Kita, *Phys. Rev. A* 66, 053610 (2002)
- [20] A. Putra, F. Salces-Carcoba, Y. Yue, S. Sugawa, I. B. Spielman, *Phys. Rev. Lett.* 124, 053605 (2020)
- [21] Y. Li, G. I. Martone, L. P. Pitaevskii, and S. Stringari, *Phys. Rev. Lett.* 110, 235302 (2013)
G. I. Martone, Y. Li, and S. Stringari, *Phys. Rev. A* 90, 041604(R) (2014)
- [22] S. K. Adhikari, *Phys. Lett. A* 388, 127042 (2021)
S. K. Adhikari, *Phys. Rev. A* 103, L011301 (2021)
- [23] S. K. Adhikari, *Physica E* 118, 113892 (2020)
- [24] H. Zhai, *Int. J. of Mod. Phys. B* 26, 1230001 (2012)
- [25] E. P. Gross, *Nuovo Cimento* 20, 454 (1961); L. P. Pitaevskii, *Zurn. Eksp. Teor. Fiz.* 40, 646 (1961) [English Transla.: *Sov. Phys. JETP* 13, 451 (1961).]
- [26] R. Ravisankar, D. Vudragović, P. Muruganandam, A. Balaž, and S. K. Adhikari, *Comput. Phys. Commun.* 259, 107657 (2020)
P. Muruganandam and S. K. Adhikari, *Comput. Phys. Commun.* 180, 1888 (2009)
D. Vudragović, I. Vidanović, A. Balaž, P. Muruganandam, S. K. Adhikari, *Comput. Phys. Commun.* 183, 2021 (2012)
- [27] E. G. M. van Kempen, S. J. J. M. F. Kokkelmans, D. J. Heinzen, and B. J. Verhaar, *Phys. Rev. Lett.* 88, 093201 (2002)
- [28] A. Crubellier, O. Dulieu, F. Masnou-Seeuws, M. Elbs, H. Knockel, and E. Tiemann, *Eur. Phys. J. D* 6, 211 (1999)
- [29] S. Gautam and S. K. Adhikari, *Phys. Rev. A* 91, 063617 (2015)
S. Gautam and S. K. Adhikari, *Laser Phys. Lett.* 12, 045501 (2015)
- [30] H. Sakaguchi, E. Ya. Sherman, and B. A. Malomed, *Phys. Rev. E* 94, 032202 (2016)